30/5/22/89 J 5 ②

Conf-890231--3

SLAC-PUB--4852

DE89 011361

THE MARKII VERTEX DRIFT CHAMBER*

J.P Alexander,[a] R.Baggs, D.Fujino, K.Hayes, C.Hoard, N.Hower, D.Hutchinson, J.A.Jaros, D.Koetke, L.A.Kowalski, C.T.Munger, T.Ohama,[b] M.L.Perl, R.Wright

Stanford Linear Accelerator Center
Stanford University, Stanford, California 94309

P.S.Drell,[a] R.Fuzesy, R.Harr, J.F.Kral, J.D.Richman,[c] B.A.Schumm, G.H.Trilling

Lawrence Berkeley Laboratory and Department of Physics
University of California, Berkeley, California 94720

W.T.Ford, D.A.Hinshaw, J.G.Smith, S.R.Wagner, P.Weber

Department of Physics
University of Colorado, Boulder, Colorado 80309

ABSTRACT

We have completed constructing and begun operating the Mark II Drift Chamber Vertex Detector. The chamber, based on a modified jet cell design, achieves 30 μm spatial resolution and < 1000 μm track-pair resolution in pressurized CO_2 gas mixtures. Special emphasis has been placed on controlling systematic errors including the use of novel construction techniques which permit accurate wire placement. Chamber performance has been studied with cosmic ray tracks collected with the chamber located both inside and outside the Mark II. Results on spatial resolution, average pulse shape, and some properties of CO_2 mixtures are presented.

Presented at the Wire Chamber Conference
Vienna, Austria, Feb. 13 – 17, 1989

---

* This work was supported by the Department of Energy, contract DE-AC03-76SF00515.

a Present address: Cornell University, Ithaca, NY 14853

b Visitor from KEK, Japan

c Present address: University of California, Santa Barbara, CA 93106

1. Introduction

The Mark II Drift Chamber Vertex Detector (DCVD) is a high precision, pressurized drift chamber which has been built to tag and study heavy flavor production at the Stanford Linear Collider (SLC)[1]. To optimize impact parameter resolution in the dense track environment at the Z^0, we use a pressurized cool gas in a modified jet cell. Several groups including our own have demonstrated ~ 30 μm spatial resolution and sub-millimeter track-pair separation in such chambers[2-4]. The task of building a large detector which fully exploits such performance is especially challenging because the electron drift velocity depends sensitively on the reduced field, the temperature, and the gas composition.

To address these problems, we adopted a novel design to achieve high mechanical precision and implemented active temperature and pressure control systems. The chamber and its readout and control systems were completed in October, 1988, and have since been thoroughly tested in a two-week cosmic ray run inside the Mark II detector[4]. Spatial and track-pair resolution with the full system reproduced our prototype results[3]. Very high wire placement accuracy was achieved, and temperature and pressure stability have been demonstrated. Determination of the distance-time relation and the off line calibration is underway.

2. Chamber description

The active volume of the DCVD extends from 5 to 17 cm radially and 55 cm axially. The chamber is divided into 10 jet cells, which are tilted with respect to the radial direction (See Fig. 1). This feature resolves the left-right ambiguity, helps in the drift velocity calibration, and ensures that no track is poorly measured along its entire length. Each cell contains an anode plane of alternating 20 μm diameter sense and 225 μm diameter potential wires sandwiched between two grid planes of 150 μm diameter wires. The [illegible] improve the sense wire electrostatic stability, improve the [illegible] isochrony, and reduce cross talk. Sense wires are spaced [illegible] apart, the grid planes are spaced 1.8 mm from the anode plane. The chamber operates at pressures up to 3 atmospheres in CO_2/C_2H_6 (92/8). Planes

of 225 μm diameter cathode wires bisect the angle between adjacent grid planes. Voltages on each cathode plane are evenly graded between -3.295 and -11.707 kV, providing a 2.3 kV/cm drift field which is uniform to better than 0.1% over two thirds of the active volume. The anode wires are run at +2.940 kV, the interspaced potential wires at ground, and the grid planes at -.480 kV. Three types of field shaping electrodes are used to grade the drift field and improve its uniformity near cell boundaries. Conducting surfaces ("skins") made of copper-clad kapton are epoxied to the inside surfaces of the inner and outer pressure cylinders. Twenty "V" shaped aluminum electrodes are placed between the anode and cathode planes and the outer skin. Guard planes containing 9 wires at the outer radius and 7 wires at the inner radius are placed between the end wires of the cathode and grid planes.

3 Mechanical Construction

In order that the impact parameter resolution not be limited by the uncertainty in wire placement, the positions of the anode wires must be known to about $\pm$ 5 microns, with somewhat looser requirements on the placement of field cage wires. With a large number of closely-spaced wires this can best be achieved by winding the wires into a small number of precise planes, which are then positioned as units within the chamber, rather than by stringing each wire individually through a positioning feedthrough. The resulting chamber geometry can thus be accurately characterized by a small number of parameters which can be measured using cosmic ray tracks.

Wire planes were wound on a pair of precision-grooved, copper-clad Invar cylinders, and then epoxied with the aid of a travelling microscope to two foundations which form the ends of the drift cell. In this way, the wires are located within a few microns of their desired positions as shown in Fig. 2. The foundations which hold the anode planes are made of stainless steel. The wires are glued to a thin piece of Macor insulator which is epoxied to the front surface of the foundation. The foundations which support the other wire planes are machined from solid Macor

blocks. The wire planes are epoxied in precise relation to a pair of conical stainless steel inserts mounted in each foundation which serve to accurately position the foundation when the completed assembly is installed in the chamber. Electrical connections are made with flexible kapton printed circuits which have been potted into pressure/HV feedthroughs (see Fig. 3). The modular construction of the jet cells permitted thorough testing and measurement of each component before its installation in the chamber.

In order to locate the foundations within the chamber, a precise matching set of conical inserts was mounted into the two positioning endplates using an Ultradex Model B precision dividing head. A pair of ball bearings, captured between the inserts of a foundation and endplate, position the foundation onto the endplate with micron-level reproducibility. The endplates were aligned on a surface table with a set of precisely cut granite blocks before being epoxied to the inner beryllium cylinder. The endplates are parallel to ± 25 μm, the relative rotation of the endplates about the chamber axis is less than ± 40 μrad. Care was taken that these endplates were not distorted by the wire tension, the gas pressure, or the stresses imposed by bolting the pressure vessel.

The gap between the grid and anode planes in the chamber demonstrates the accuracy of the final placement of the wire planes. All but one of the twenty anode-grid gaps are within 25 microns of their nominal 1.8mm (see Fig. 4).

Several mechanical problems were encountered during construction. A number of the Macor foundations either developed surface cracks, or shed small conical pieces around the threaded inserts used to pull the wire planes up to tension. Macor is brittle and fragile and required considerable care in handling. The mating surface of the anode foundations and supporting endplate were too small to guarantee accurate positioning. Adequate reproducibility was obtained only after considerable testing and rejection of anode foundations. The stress induced from bending the 'V' shaped aluminum field shaping electrodes caused some of them to deform out of tolerance over a period of several weeks. This was not consid-

ered serious enough to warrant disassembling the chamber for repair. Finally, the kapton printed circuits must be flexed to assemble the chamber, and some copper traces fatigued and broke, typically where traces followed a sharp corner instead of a smooth curve. Epoxying additional layers of kapton on the surfaces of the printed circuits made them more tolerant to mechanical stress.

4. High voltage system

The high voltage system is designed to supply accurate and stable voltages to all chamber electrodes, to monitor chamber voltages and currents, and to protect the chamber by quickly removing voltages if excess current is detected. A block diagram is shown in Fig. 5.

A single high voltage supply powers the 10 resistor divider chains which supply the 68 voltages required for the cathode and field shaping electrodes in each cell. All other voltages are obtained directly from separate supplies. Current monitors in each high voltage channel trigger protection circuitry that within a few milliseconds switches all high voltage lines into 80 kΩ discharge resistors when excess current is detected. Filters located near the chamber remove high frequency noise and break ground loops.

The voltage distribution for each sense plane is segmented into 4 buses of 10 adjacent wires that are powered by a single supply. Each wire is connected to the bus through a 25 MΩ resistor. Preamplifiers are coupled to the anode wires through 100 pF capacitors which isolate the high voltage and minimize the energy available to a spark discharge. Each grid plane is connected to a separate voltage bus. All the grid planes are powered from a single supply. The grid and anode trip levels are 250 and 100 nanoamps respectively.

Voltages are set to a few parts in 10^4 via a computer controlled feedback loop. A FLUKE model 8506A digital multimeter with 5 *ppm* accuracy samples the individually calibrated monitor outputs of the high voltage supplies. Sixteen bit DAC's generate the control voltages for the supplies.

To obtain voltage ratios accurate to a few parts in 10^4, resistors for the divider

chains were individually measured and grouped on the basis of resistance and temperature coefficient. The total chain resistance is 143.38 MΩ. For a drift field of 2.3 kV/cm, the voltage at the top of the chain is 12.6 kV, and the chain current is about 88 μamp. Chamber leakage currents are measured by comparing the voltages near the top and bottom of the chain against an identical reference chain. Typical cathode plane leakage currents are less than 10 namp. Monitor circuits trip the system if the difference current at the top or bottom of the chain exceeds set limits, typically 5 and 0.25 μamp at the top and bottom respectively.

Flexible kapton printed circuits connect planes of chamber wires to high density multi-pin connectors located on the outside of the pressure feedthrough (see Fig. 6). A protective layer of 50 μm thick kapton bonded to each side of the circuitry ensures high trace-to-trace dielectric strength and resistivity. Additional layers of kapton were epoxied to the printed circuits to prevent high voltage discharges, and to make the circuitry tolerant to stress. The resistor divider cards, pressure feedthroughs and connectors were all potted in epoxy. Very thorough mixing, elimination of air bubbles by vacuum pumping, and heating surfaces to remove absorbed water guaranteed good dielectric strength in the epoxy[5]. It was also necessary to remove all traces of alcohol, which was used extensively in cleaning components, to guarantee that the epoxy cured properly.

5. Gas and temperature control systems

The chamber gas, CO_2 with an 8% admixture of C_2H_6 to provide quenching, is run in the unsaturated regime (E/p = 77 kV/cm/atmos) where it exhibits both low electron diffusion and a slow drift velocity (5.7 μm/nsec). The gas flows at a rate of 1 to 2 scfh and is not recirculated. The gas is mixed commercially and supplied in quantities sufficient for one year of chamber operation, which ensures that the gas composition is stable. The gas system (Fig. 7) was built using brass compression fittings and oxygen free high conductivity copper tubing, which was hydrogen fired to remove any remaining volatile contaminants. To achieve electron lifetimes above 30 μsec (which corresponds to a 25% loss in pulse height over a 5 cm

drift) the oxygen level must be less than 2 ppm. Oxisorb filters are used to reduce the oxygen content of the gas to less than 0.2 ppm, although leaks increase this to about 1 ppm in the chamber. The leak rate for the chamber at 3 atmospheres pressure is less than 0.01 psi/hour.

The gas quality is monitored using a test chamber which can measure the drift velocity and electron lifetime of the gas as it returns from the chamber. The oxygen content of the gas is measured using a Teledyne model 316 Oxygen Analyzer which has an accuracy of ±0.2 ppm. Pressure measurement and control to ±0.01 psi (0.7 mbar) is achieved using a Datametrics Model 1501 pressure controller and Type 590 pressure transducer.

CO_2/C_2H_6 is relatively radiation hard. In a prototype chamber irradiated with an Fe^{55} source, we observed a 50% loss in gain after an accumulated charge of 0.6 C/cm. The loss of gain was due to silicon-containing deposits on the sense wires.

Drift velocity in CO_2/C_2H_6 depends sensitively on temperature, as shown in Fig. 9. An active temperature control system is used to compensate for the 20 Watts of heat from the preamplifiers and resistor cards and 2.3 °C diurnal variations in the ambient temperature. Water from a Haake N2-R computer-controlled water bath is pumped through a 1/4" diameter aluminum tube that is soldered to the inner and outer radii of each pressure head and welded in a spiral around the outer shell of the chamber. The flow, at a rate of about 30 gallons/hour, was chosen to be just above the onset of turbulence. Forty-eight thermistors monitor the temperatures of the gas volume, pressure heads, inner and outer shells, and electronics cages, with their temperatures written to tape every four minutes. The bath temperature is adjusted by the online computer to hold the chamber temperature constant. In this way, temperatures in the chamber are held uniform and stable to ± 0.1 °C.

6. Data readout system

A linear, 6 bit, 100 MHz Flash ADC (FADC) system is used for chamber readout. Preamplifier cards, 1 per cell, mount just outside the pressure endplate and plug into the anode plane feedthrough connectors. Each card contains 38 channels of a fast, charge-sensitive, hybrid amplifier[6] which has a 40 nsec integration time. The preamplifiers connect by 30 feet of 50 ohm coaxial cable to postamplifiers which amplify and filter the wire signals. Three stages of pole zero filter compensate for the integration time constant and remove the $1/t$ positive ion tail. Each postamplifier connects to the FADCs through a 100 foot individually shielded twisted pair cable. The overall electronic gain has been set so that the root-mean-square thermal noise is about half of a least count. The gas gain is set to about $5 \cdot 10^4$ in order to obtain the proper signal levels at the FADC. The crosstalk between any pair of channels is less than one percent for hits from the uniform field region of the chamber.

The 16-channel FADC modules[7] reside in two FASTBUS crates. The memory depth of each channel is 1024 samples. The FADC sample clock is provided by a single crystal oscillator[8] (stable to $\pm 2 \cdot 10^{-7}$/week) which is phase-locked to the SLC timing signal. One SLAC-Scanner Processor (SSP) module[9] in each crate reads and processes the FADC data, providing hit recognition, zero suppression and time and charge determination, and formats the raw and processed data for later use. Typical processing times in an SSP are about 1 msec/track.

A calibration system monitors channel pedestals, gains, and timing offsets. Pedestals are stable to $\pm$ 1/3 of an FADC least count.

7. Cosmic ray test results

The chamber and its subsystems were completed in October, 1988, and subsequently tested with cosmic rays, including a period of running inside the Mark II. The chamber was operated in both 2 atmospheres of pure CO_2 and 3 atmospheres of CO_2/C_2H_6 (92/8); for both runs the electron lifetime was about 40 μsec. Data

from these two runs are presented below. A cosmic ray event (from the pure CO_2 running), which produces a delta ray in the inner wall of the chamber, is shown in Fig. 10.

The spatial resolution was studied using triplets of adjacent wires by forming the quantity $r \approx \frac{1}{\sqrt{6}} \cdot w \cdot (2T_i - T_{i+1} - T_{i-1})$ where T_i is the hit time of wire i. The drift velocity w was determined using tracks which cross the cathode or anode planes. Triplets from tracks making an angle larger than 30° to the anode plane were not used. Hits within two mm of the anode or cathode planes were also rejected. To determine the resolution, the r distributions were binned by drift distance D and fit to gaussians. Fig. 11 shows the squared resolution versus D for both runs. The data have been fit to the function $\sigma_r^2 = \sigma_o^2 + S \cdot D$ where σ_o is a constant and S accounts for electron diffusion. The resolution is dominated by diffusion. The fit values of σ_o and S (Table 1) are in good agreement with our prototype results[3]. The resolution is found to be largely independent of the angle between the track and anode plane. The timing algorithm used in this analysis is an exponentially weighted centroid of FADC samples:

$$t = \frac{\sum_i \alpha^i \cdot p_i \cdot t_i}{\sum_j \alpha^j \cdot p_j}$$

where t_i and p_i are the time and pulse height for sample i, and $\alpha < 1$ varies linearly with drift distance and is adjusted to optimize the resolution (Table 1).

The average pulse shape provides a measure of the chamber double-track resolution which is independent of pattern recognition algorithms and fake hit rates. This distribution is the average of the raw FADC waveforms appropriately shifted to start at the time prescribed by the hits on the two adjacent wires. Fig. 12a shows the average pulse shape for the CO_2/C_2H_6 data. The leading edge of the average pulse is determined by electron diffusion in the gas. Fig. 12a shows the average pulse shape for two ranges of ϕ, the track angle with respect to the anode plane. Significant lengthening of the pulse is observed when ϕ exceeds about 25°.

For $\phi < 25\ ^{o}$, the non-isochrony of the cell is primarily responsible for the shape of the trailing edge. In pure CO_2, late-arriving pulses significantly increase the size and extent of the tail associated with the trailing edge. This effect is illustrated in Fig. 12b which shows the average pulse shapes in CO_2 and CO_2/C_2H_6 with a logarithmic vertical scale.

The track-pair resolution depends on the specific algorithms employed to recognize hits in the FADC data and to determine hit times. However, it is clear from Fig. 12a that for tracks which originate in the SLC interaction region and therefore have small angles to the anode plane, the track-pair resolution will be better than 1 mm.

Vertex chamber ionization loss (dE/dX) measurements will be used in conjunction with measurements in the Mark II central tracking chamber[10] to identify charged particles. A preliminary analysis of the cosmic ray data shows the dE/dx resolution to be about 9 percent in CO_2 at 2 atmospheres.

8. Conclusion

The new drift chamber vertex detector for the Mark II detector has been completed. Tests using cosmic rays show that the chamber achieves 30 μm spatial resolution and < 1000 μm track-pair resolution. Studies of the impact parameter resolution are in progress. Final installation in the Mark II awaits completion of an SLC-compatible beam pipe and is expected by Fall, 1989.

Acknowledgements

We greatly appreciate the work of the engineers and technicians without whom this chamber could not have been built. In particular we thank L. Barker, B. Leonard, T. Nakashima, and R. Stickley. This work was supported in part by the Japanese Ministry of Education, Science and Culture through the Japan U.S.A. Cooperative Research Project on High Energy Physics.

REFERENCES

1 K. G. Hayes, Nucl. Instr. and Meth. **A265**, (1988) 60. J. Jaros, Vertex Detectors: Proceedings of the Erice Workshop for the INFN Eloisatron Project, ed. by F. Villa (1988) 37

2 H. Anderhub *et al.*, Nucl. Instr. and Meth. **A265** (1988) 50; H. Anderhub *et al.*, Nucl. Instr. and Meth. **A252** (1986) 357; V. Commichau *et al.*, Nucl. Instr. and Meth. **A235** (1985) 267; D. Bettoni *et al.*, Nucl. Instr. and Meth. **A236** (1985) 237; S. Bobkov *et al.*, Nucl. Instr. and Meth. 226 (1984) 375.

3 J. Alexander *et al.*, Nucl. Instr. and Meth. **A252**, (1986) 350.

4 G. Abrams *et al.*, SLAC-PUB-4558 submitted to Nucl. Instr. and Meth. **A**.

5 Henkel Corporation Versamid 140 and Shell Epon 815 or Epon 826, 50/50 by weight, was the epoxy used everywhere in the chamber except for high load joints in the pressure vessel, where we used Dexter Hysol EA 9309 NA.

6 BNL hybrid IO-364.

7 L. Barker SLAC-PUB 4757, D. Bernstein *et al.*, IEEE Trans. Nucl. Sci. 33 (1986) 86.

8. Berkeley Nucleonics model C-1000.

9. H. Brafman *et al.*, IEEE Trans. N.S. 32 (1985) 436.

10. See contribution to this conference by D. Coupal *et al.*

FIGURE CAPTIONS

Fig. 1. Cross-sectional view of the Mark II vertex chamber

Fig. 2. Measured deviations out of the plane for each wire in a completed sense wire plane.

Fig. 3. End view of chamber before installation into pressure vessel. The Macor foundation blocks, kapton artworks, pressure feedthroughs, and anode support structure are shown.

Fig. 4. Deviation of the spacing between each grid and anode plane from the design value for grid planes on Macor blocks a) which do not also support cathode planes and b) which do also support cathode planes

Fig. 5. Block diagram of the high voltage system.

Fig. 6. Schematic view of the Macor foundation block, kapton artwork, pressure feedthrough, and high voltage connector

Fig. 7. Schematic diagram of the chamber gas system

Fig. 8. Inverse electron lifetime as a function of O_2 concentration measured with a prototype chamber.

Fig. 9. Drift velocity as a function of temperature. The fractional change in the drift velocity (at 300°K) is determined from the linear fit to the data

Fig. 10. Display of a cosmic ray event which produces a delta ray from a run when the vertex chamber (filled with 2 atmospheres of CO_2) was installed in the Mark II detector. Cathode planes are shown as solid lines

Fig. 11. Squared spatial resolution as a function of drift distance to the anode plane.

Fig. 12a. Average pulse shape of hits on cosmic ray tracks for two intervals of the track angle ϕ to the anode plane.

Fig. 12b. Average pulse shape of hits on cosmic ray tracks in 3 atmospheres of CO_2/C_2H_6 and 2 atmospheres in pure CO_2

Table 1. Results of the fit to the measured spatial resolution as a function of drift distance D, $\sigma_r^2 = \sigma_0^2 + D \cdot S$. The optimized weight α of the hit timing algorithm (see text) is also listed.

Gas	Pressure (Bar)	σ_0 (μm)	S (μm/$\sqrt{\text{cm}}$)	α
CO_2	2	$19.9 \pm .8$	$36.9 \pm .4$	$.53 \pm .061 \cdot D$ (cm)
CO_2/C_2H_6	3	$20.3 \pm .6$	$26.2 \pm .3$	$.55 \pm .031 \cdot D$ (cm)

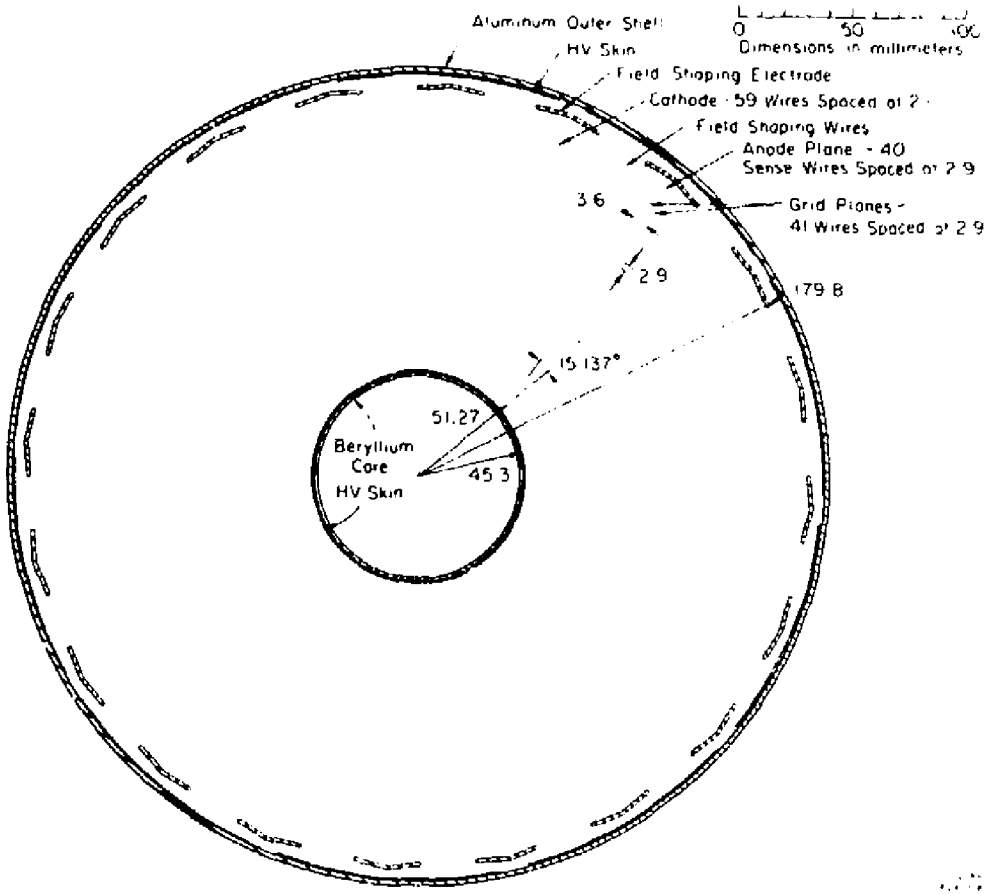
Aluminum Outer Shell
HV Skin
Field Shaping Electrode
Cathode - 59 Wires Spaced at 2
Field Shaping Wires
Anode Plane - 40
Sense Wires Spaced at 2 9
Grid Planes -
41 Wires Spaced at 2 9
3 6
2 9
179 8
15 137°
51.27
45 3
Beryllium
Core
HV Skin
0
50
Dimensions in millimeters

Fig. 1

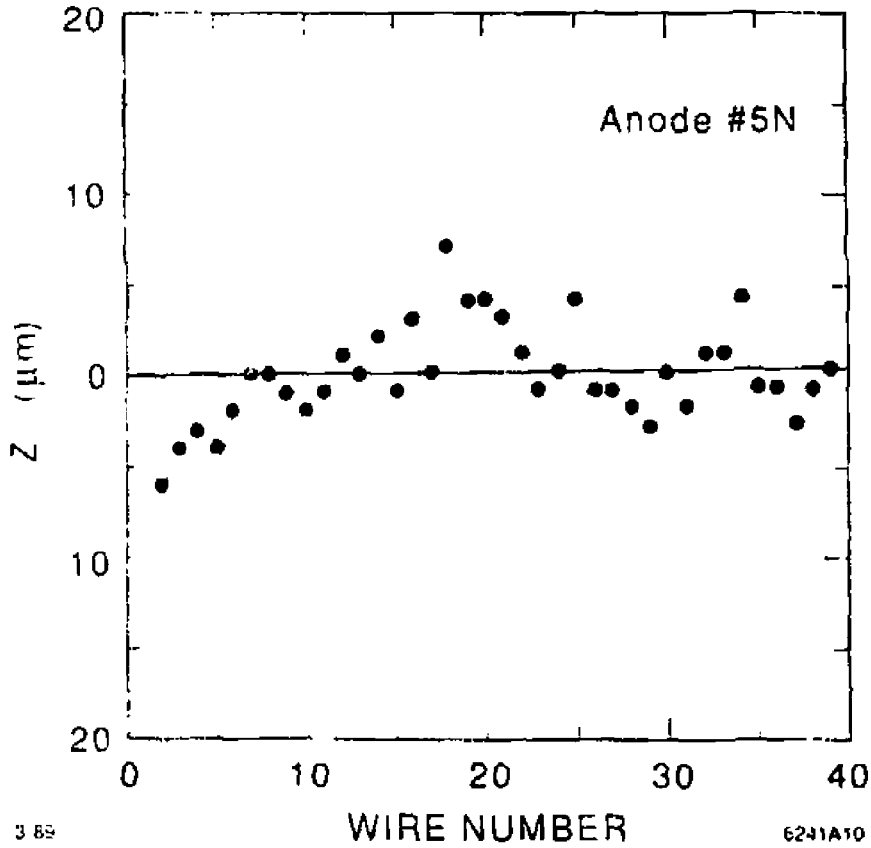

Fig. 2

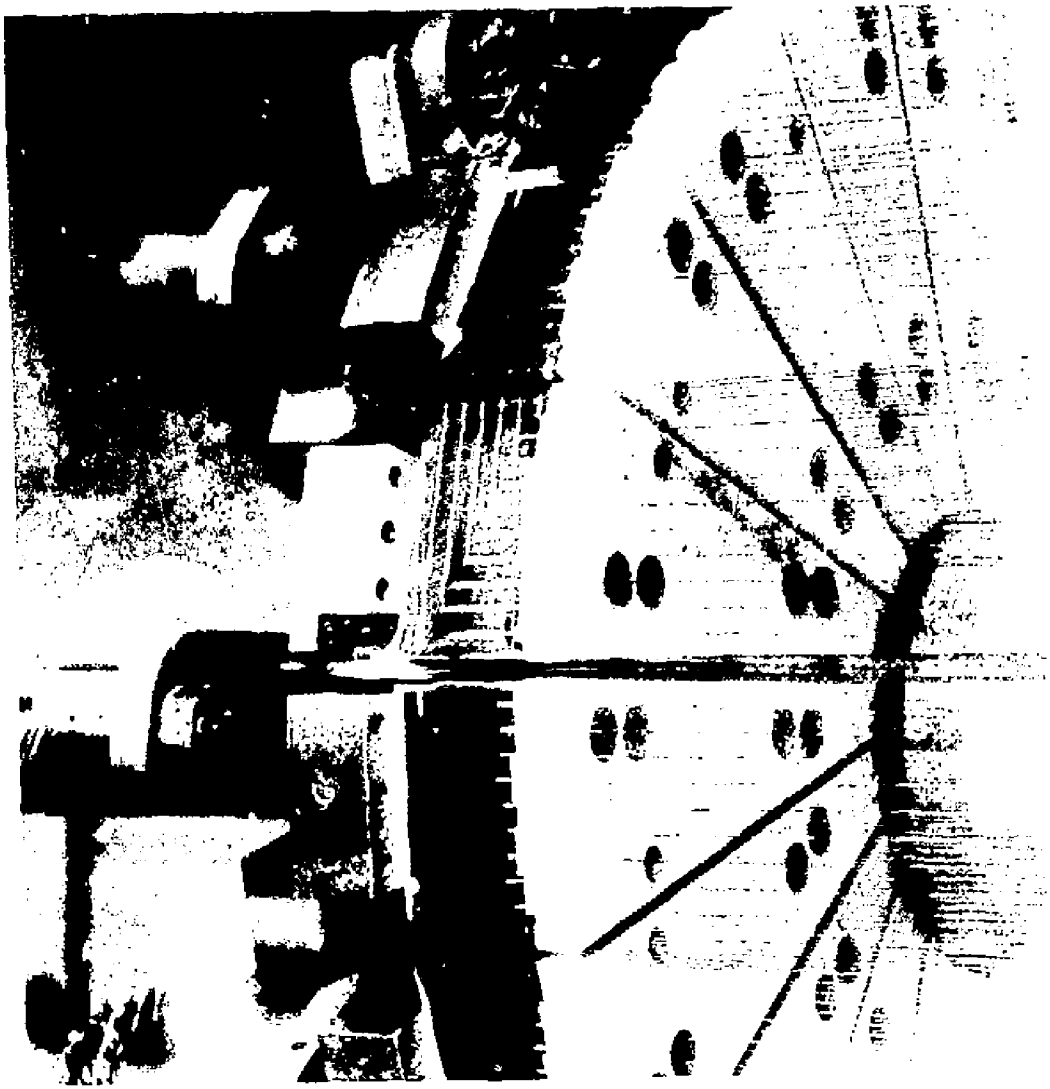

Fig. 3

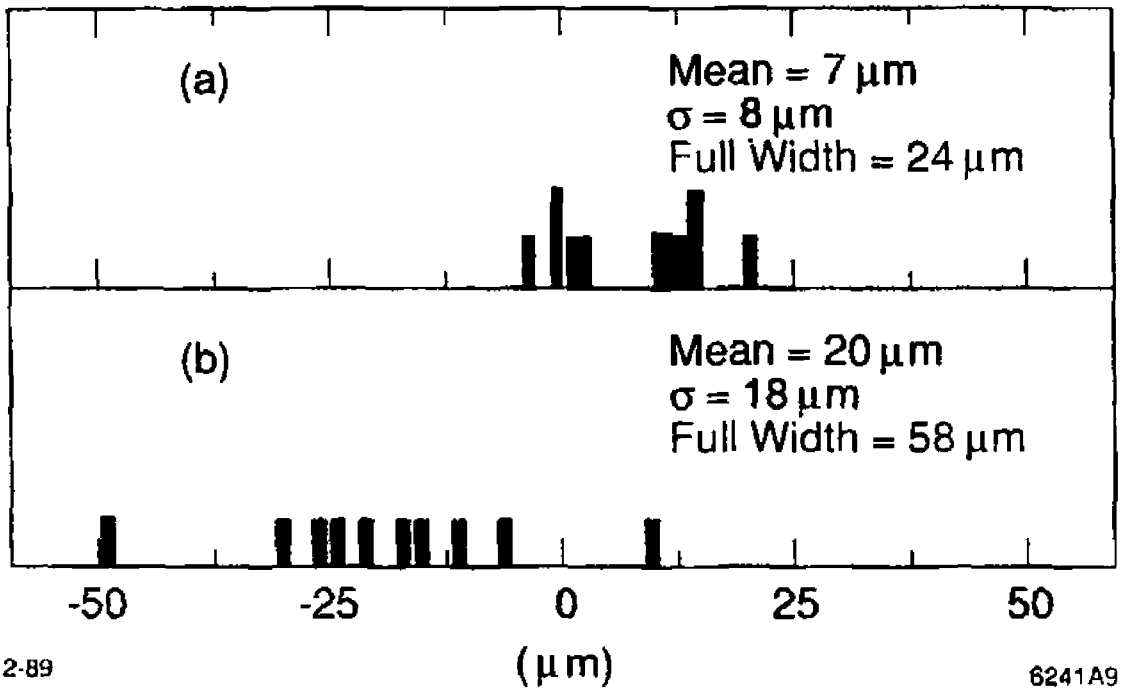
(a)
Mean = 7 μm
σ = 8 μm
Full Width = 24 μm
(b)
Mean = 20 μm
σ = 18 μm
Full Width = 58 μm
-50
-25
0
25
50
(μm)
2-89
6241A9

Fig. 4

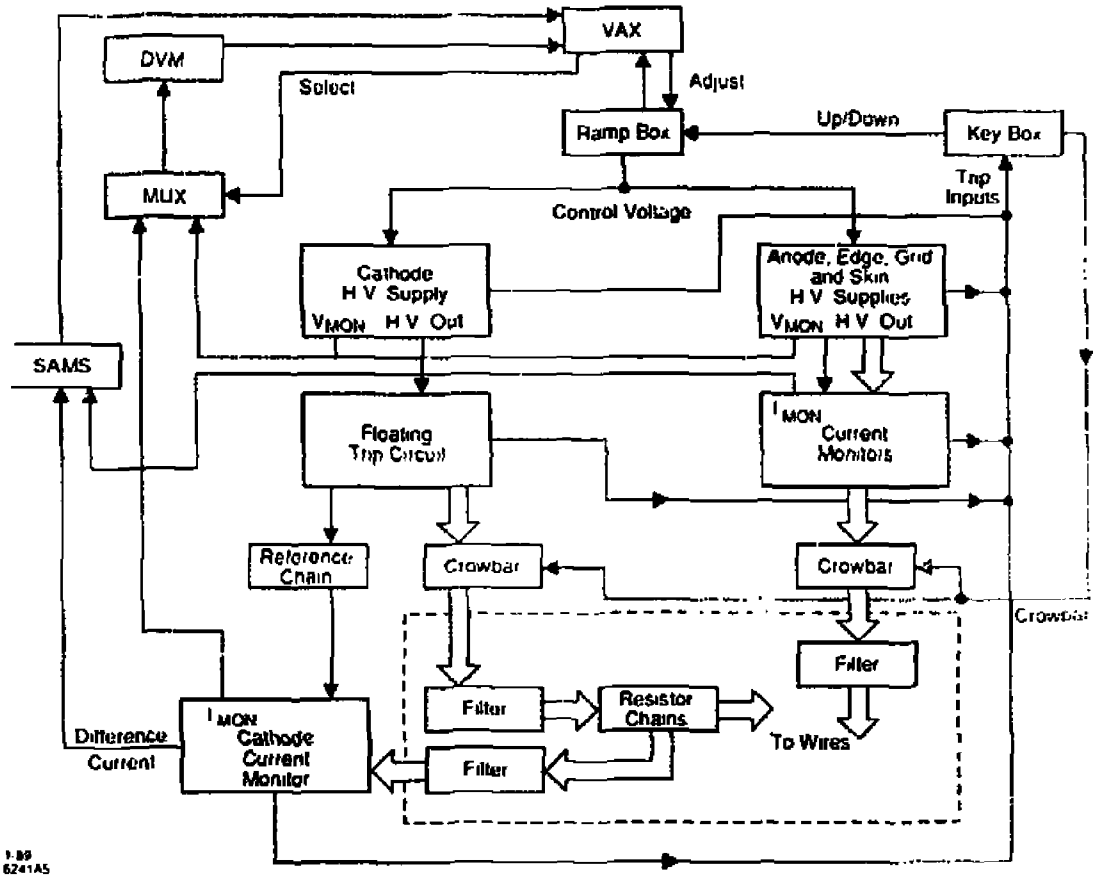
VAX
DVM
Select
Adjust
Ramp Box
Up/Down
Key Box
MUX
Trip Inputs
Control Voltage
Cathode H V Supply
VMON H V Out
Anode, Edge, Grid and Skin H V Supplies
VMON H V Out
SAMS
Floating Trip Circuit
IMON Current Monitors
Reference Chain
Crowbar
Crowbar
Crowbar
Filter
Filter
Resistor Chains
To Wires
Filter
Difference Current
IMON Cathode Current Monitor
1-89
6241A5

Fig. 5

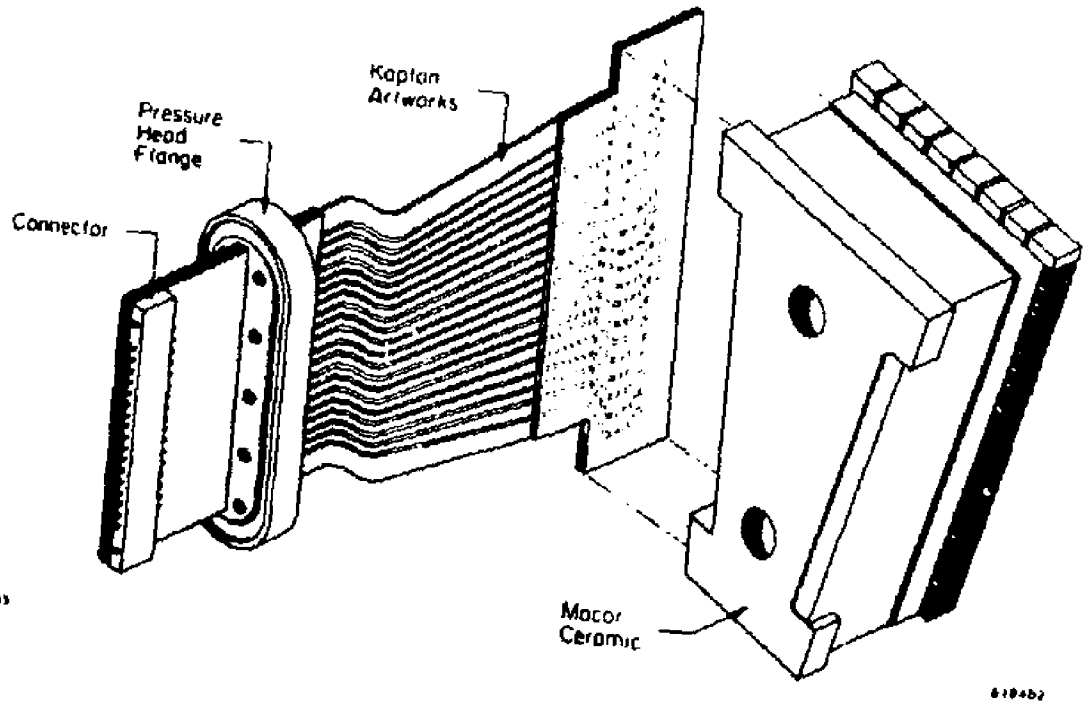
Kapton
Artworks
Pressure
Head
Flange
Connector
Macor
Ceramic

Fig. 6

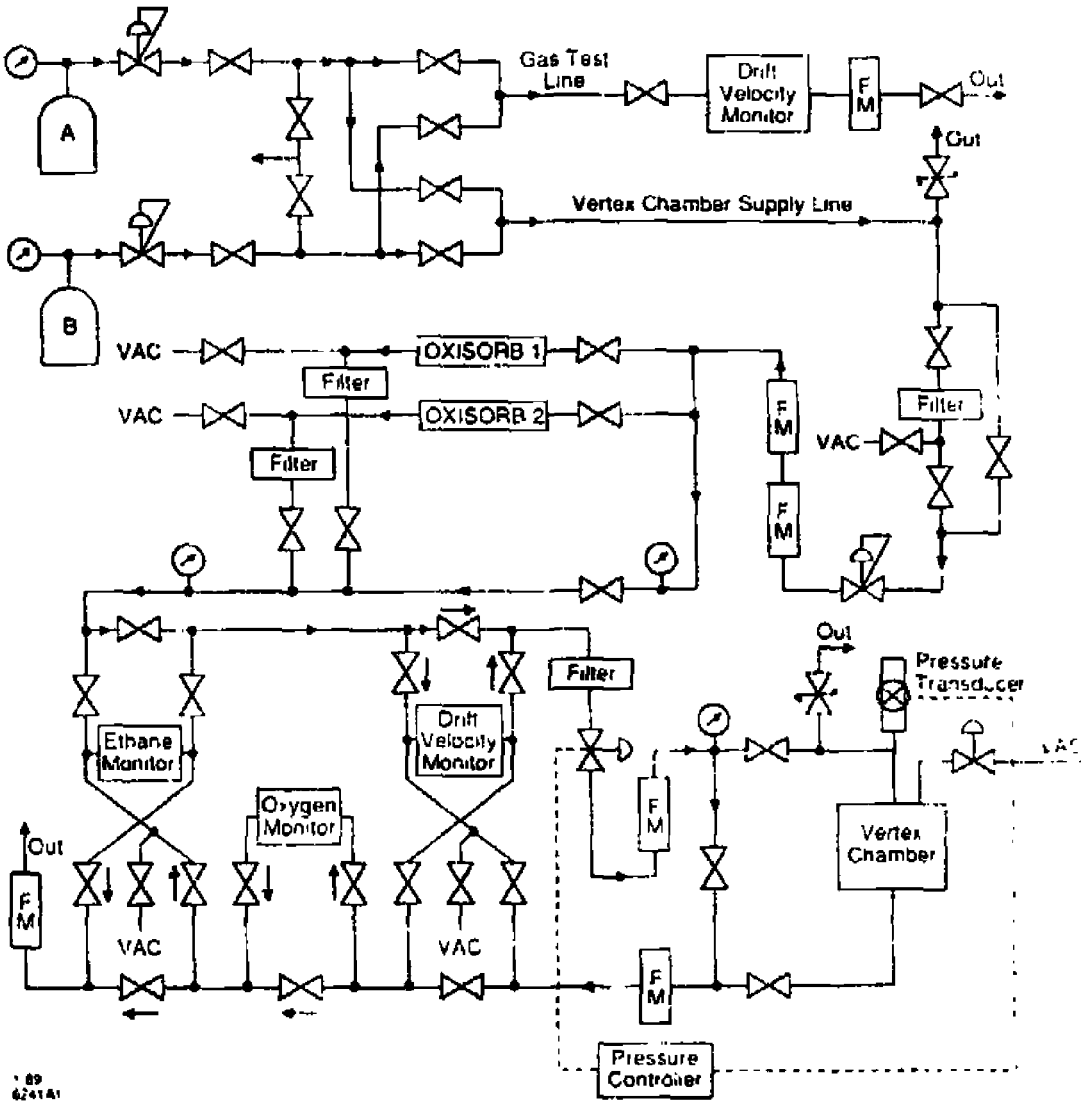
A
B
Gas Test Line
Drift Velocity Monitor
F M
Out
Vertex Chamber Supply Line
VAC
OXISORB 1
OXISORB 2
Filter
Ethane Monitor
Oxygen Monitor
Drift Velocity Monitor
Pressure Transducer
Vertex Chamber
Pressure Controller

Fig. 7

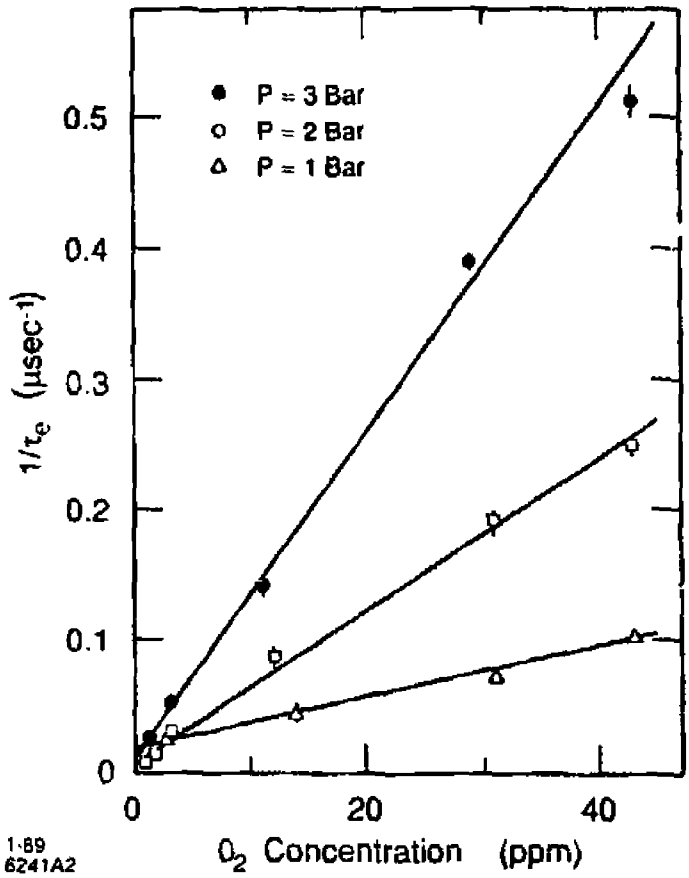
P = 3 Bar
P = 2 Bar
P = 1 Bar
0.5
0.4
0.3
0.2
0.1
0
1/τe (μsec-1)
0
20
40
O2 Concentration (ppm)
1-89
6241A2

Fig. 8

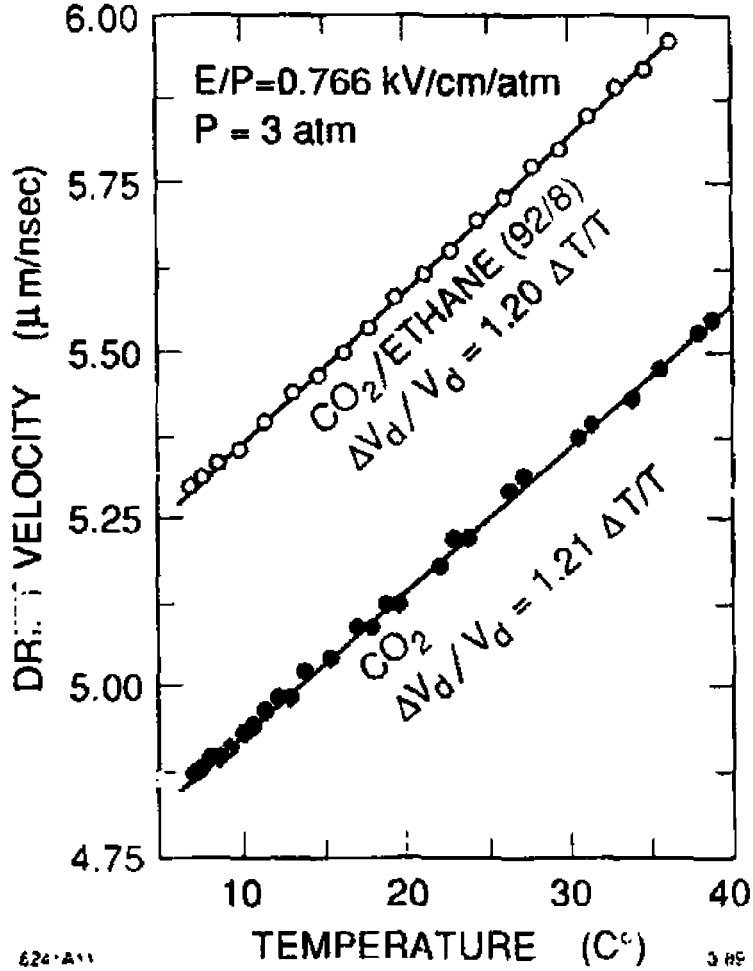
6.00
5.75
5.50
5.25
5.00
4.75
E/P=0.766 kV/cm/atm
P = 3 atm
CO2/ETHANE (92/8)
ΔVd/ Vd = 1.20 ΔT/T
CO2
ΔVd/ Vd = 1.21 ΔT/T
VELOCITY (μm/nsec)
10
20
30
40
TEMPERATURE (C°)

Fig. 9

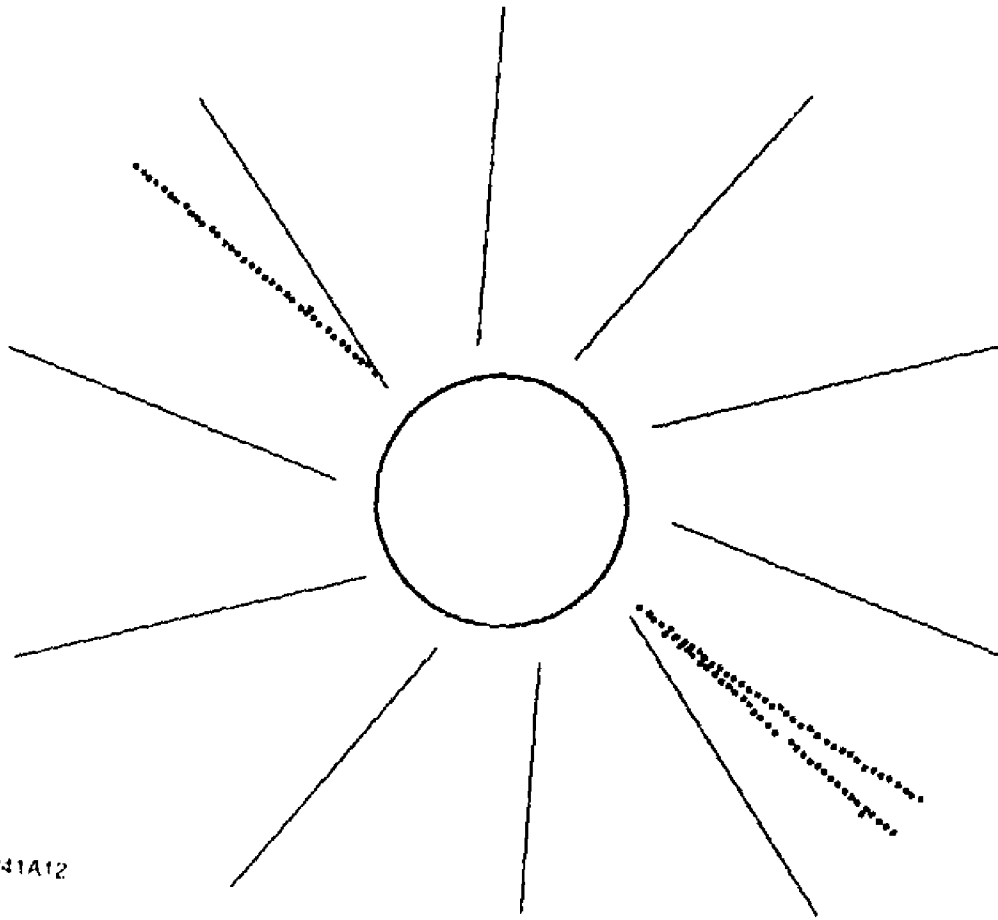

Fig. 10

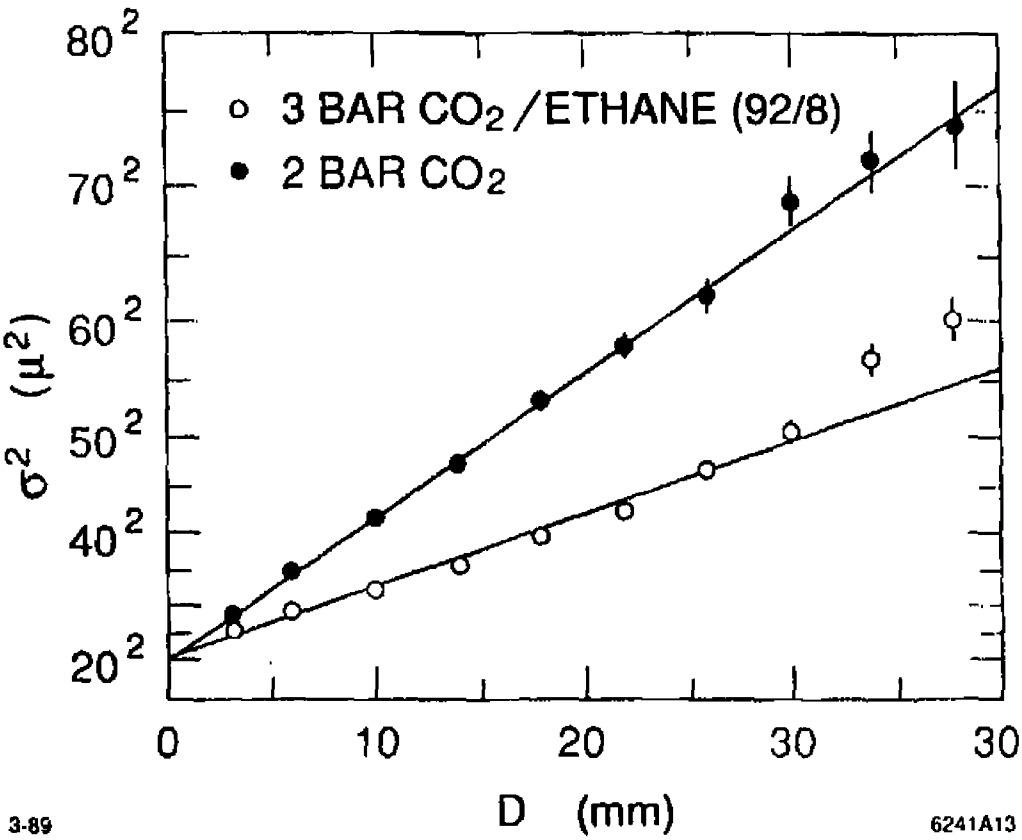
80 2
70 2
60 2
50 2
40 2
20 2
σ2 (μ2)
3 BAR CO2 /ETHANE (92/8)
2 BAR CO2
0
10
20
30
30
D (mm)
3-89
6241A13

Fig 11

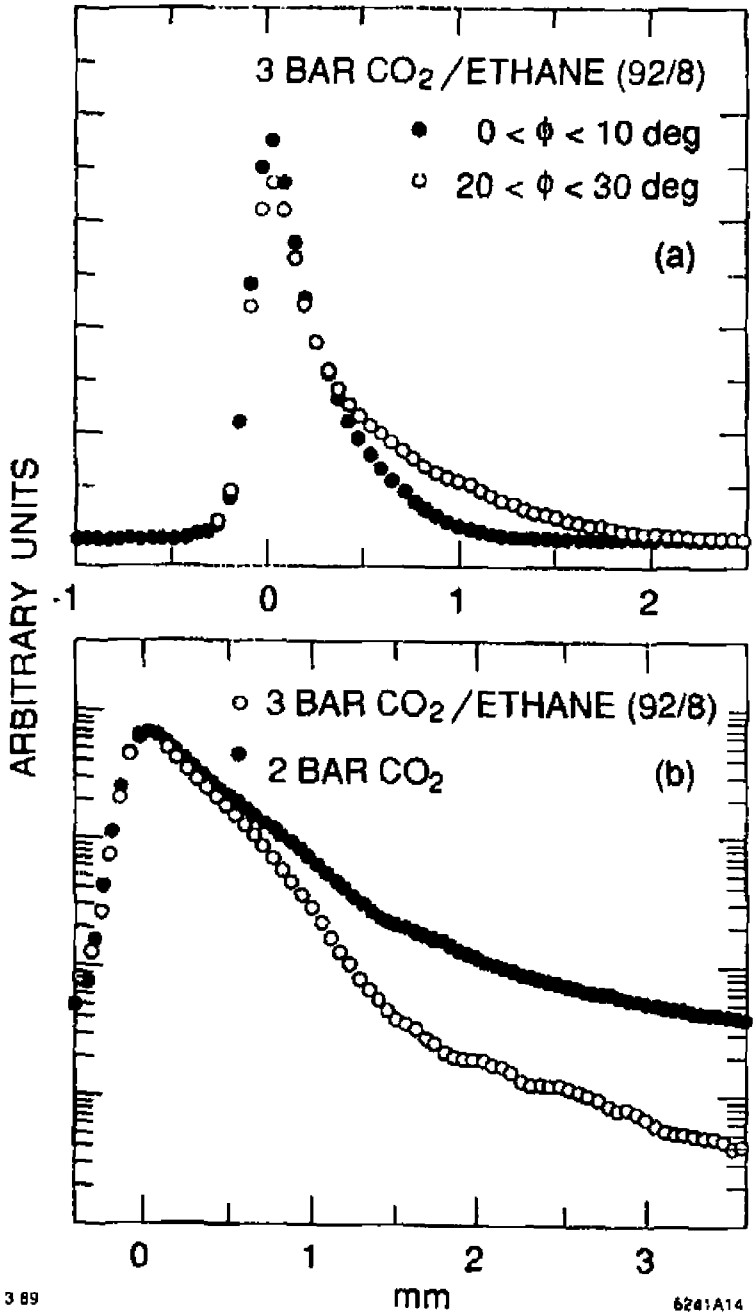

Fig. 12

GPO 687-090/19125

DISCLAIMER